Journal of Structural Biology 175 (2011) 300–310

Contents lists available at ScienceDirect

Journal of Structural Biology

journal homepage: www.elsevier.com/locate/yjsbi

Conformational change upon product binding to *Klebsiella pneumoniae* UDP-glucose dehydrogenase: A possible inhibition mechanism for the key enzyme in polymyxin resistance

Ying-Yin Chen [a,b,1], Tzu-Ping Ko [a,1], Chun-Hung Lin [a,b], Wei-Hung Chen [a], Andrew H.-J. Wang [a,b,*]

[a] Institute of Biological Chemistry, Academia Sinica, Taipei 115, Taiwan
[b] Institute of Biochemical Sciences, National Taiwan University, Taipei 106, Taiwan

ARTICLE INFO

Article history:
Received 3 January 2011
Received in revised form 22 March 2011
Accepted 14 April 2011
Available online 23 April 2011

Keywords:
X-ray crystallography
Allosteric inhibition
NAD-dependent oxidoreductase

ABSTRACT

Cationic modification of lipid A with 4-amino-4-deoxy-L-arabinopyranose (L-Ara4N) allows the pathogen *Klebsiella pneumoniae* to resist the antibiotic polymyxin and other cationic antimicrobial peptides. UDP-glucose dehydrogenase (Ugd) catalyzes the NAD^+-dependent twofold oxidation of UDP-glucose (UPG) to produce UDP-glucuronic acid (UGA), a requisite precursor in the biosynthesis of L-Ara4N and bacterial exopolysaccharides. Here we report five crystal structures of *K. pneumoniae* Ugd (*Kp*Ugd) in its apo form, in complex with UPG, UPG/NADH, two UGA molecules, and finally with a C-terminal His_6-tag. The UGA-complex structure differs from the others by a 14° rotation of the N-terminal domain toward the C-terminal domain, and represents a closed enzyme conformation. It also reveals that the second UGA molecule binds to a pre-existing positively charged surface patch away from the active site. The enzyme is thus inactivated by moving the catalytically important residues C253, K256 and D257 from their original positions. Kinetic data also suggest that *Kp*Ugd has multiple binding sites for UPG, and that UGA is a competitive inhibitor. The conformational changes triggered by UGA binding to the allosteric site can be exploited in designing potent inhibitors.

1. Introduction

The opportunistic pathogen *Klebsiella pneumoniae* can cause urinary tract and blood stream infections, as well as severe pneumonia with a high rate of mortality and morbidity (Podschun and Ullmann, 1998). It is emerging as a major causative agent of multi-drug resistant infections and pyogenic liver abscess frequently complicated by metastatic meningitis or endophthalmitis (Fang et al., 2004; Wu et al., 2009). Expression of two essential virulence factors, capsular polysaccharide (CPS) and lipopolysaccharide (LPS), in *K. pneumoniae* clinical isolates (Huh et al., 2004) allows it to escape from host innate immune responses (Easley et al., 2007). The LPS modifications with 4-amino-4-deoxy-L-arabinopyranose (L-Ara4N) further confer *K. pneumoniae* resistance to the antibiotic polymyxin (Helander et al., 1996), a member of cationic antimicrobial peptides (CAMPs). Functioning as a key component of the innate immune system (Sommer et al., 2004), CAMPs act by binding to the negatively charged lipid A of LPS on the bacterial cell surface, leading to membrane permeabilization and cell death (Burtnick and Woods, 1999; Gatzeva-Topalova et al., 2005; Princivalle and de Agostini, 2002). In order to evade the bactericidal action of CAMPs, some Gram-negative bacteria have developed mechanisms to modify the phosphate group of lipid A with the positively charged sugar L-Ara4N (Burtnick and Woods, 1999; Guo et al., 1997; Princivalle and de Agostini, 2002). By reducing the surface negative charge, such modification decreases the binding affinity and results in the resistance to CAMPs (Ordman and Kirkwood, 1977a). In *K. pneumoniae* CG43, polymyxin B (PXB) resistance was demonstrated to be correlated to the expression of UDP-glucose dehydrogenase (Ugd; EC 1.1.1.22), a LPS modification enzyme involved in L-Ara4N biosynthesis (Cheng et al., 2010).

Ugd belongs to a small group of NAD^+-dependent 4-electron oxidoreductases and catalyzes the conversion of UDP-glucose (UPG) to UDP-glucuronic acid (UGA), the initial step of the L-Ara4N biosynthesis pathway (Fig. S1) (Breazeale et al., 2005; Huh et al., 2004). UGA also serves as a precursor for synthesis of bacterial antiphagocitic CPS, colanic acid (M-antigen), plant cell walls, and mammalian glycosaminoglycans (Hung et al., 2007; Lacour et al.,

Abbreviations: CAMP, cationic antimicrobial peptide; CPS, capsular polysaccharide; L-Ara4N, 4-amino-4-deoxy-L-arabinopyranose; LPS, lipopolysaccharide; PXB, polymyxin B; UGA, UDP-glucuronic acid; Ugd, UDP-glucose dehydrogenase; UPG, UDP-glucose.

* Corresponding author at: Institute of Biological Chemistry, Academia Sinica, Taipei 115, Taiwan. Fax: +886 2 2788 2043.
E-mail address: ahjwang@gate.sinica.edu.tw (A.H.-J. Wang).

[1] These authors contributed equally to this work.

1047-8477/$ - see front matter © 2011 Elsevier Inc. All rights reserved.
doi:10.1016/j.jsb.2011.04.010

2008), and it is critical to bacterial virulence (Jiang et al., 2010) as required for the biosynthesis of extracellular polysaccharide. Mutations in the *ugd* gene of *Xanthomonas campestris* lead to loss of pathogenicity (Burtnick and Woods, 1999). In other pathogenic bacteria like *Burkholderia cenocepacia* (Gatzeva-Topalova et al., 2005) and *B. pseudomallei* (Burtnick and Woods, 1999), insertion mutagenesis studies showed that *ugd* is essential for viability and PXB resistance. Moreover, *ugd* deletion in *Pseudomonas aeruginosa* increased its susceptibility to PXB, chloramphenicol, cefotaxime, and ampicillin (Hung et al., 2007). A recent report on *Proteus mirabilis* showed that the expression of Ugd can be induced by PXB (Jiang et al., 2010). Therefore, limiting UGA availability by inhibiting Ugd activity may represent a strategy against bacterial infections.

The reaction catalyzed by Ugd is outlined in Fig. 1. Kinetic studies have been reported for the bovine (Ridley and Kirkwood, 1973), streptococcal (Campbell et al., 1997), *Arabidopsis thaliana* (Thompson et al., 1994) and human (Easley et al., 2007) enzymes. The streptococcal Ugd follows a bi-uni-uni-bi ping-pong mechanism in which UPG is bound first and UGA is released last (Campbell et al., 1997; Ordman and Kirkwood, 1977b). The proposed mechanism involves an aldehyde intermediate covalently bound to a lysine residue, nucleophilic attack of an active-site cysteine on the aldehyde, and irreversible hydrolysis of the thioester intermediate (Campbell et al., 2000; Ge et al., 1998; Ordman and Kirkwood, 1977a; Ridley and Kirkwood, 1973). This cysteine residue is conserved across all species and essential for the second step of oxidation (Ge et al., 2004; Sommer et al., 2004). Mutation of strictly conserved active-site residues in human Ugd, which correspond to K197, C253, K256, D257 and K307 in *Kp*Ugd (Fig. S2), revealed their functional importance (Easley et al., 2007; Sommer et al., 2004). On the other hand, Ugd activity is competitively inhibited by UGA in a feedback regulation for making various UDP-sugars in plants (Campbell et al., 1997; Dalessandro and Northcote, 1977; Thompson et al., 1994), while UPG exhibits slight allosteric effects in *Streptococci*, *P. aeruginosa* and *B. cenocepacia* (Campbell and Tanner, 1997; Campbell et al., 1997; Hung et al., 2007).

The X-ray structures of Ugd from *Streptococus pyogenes* (*Sp*Ugd; PDB codes: 1DLI and 1DLJ) (Campbell et al., 2000), *Porphyromonas gingivalis* (*Pg*Ugd; PDB code: 3GG2), *Caenorhabditis elegans* (*Ce*Ugd;

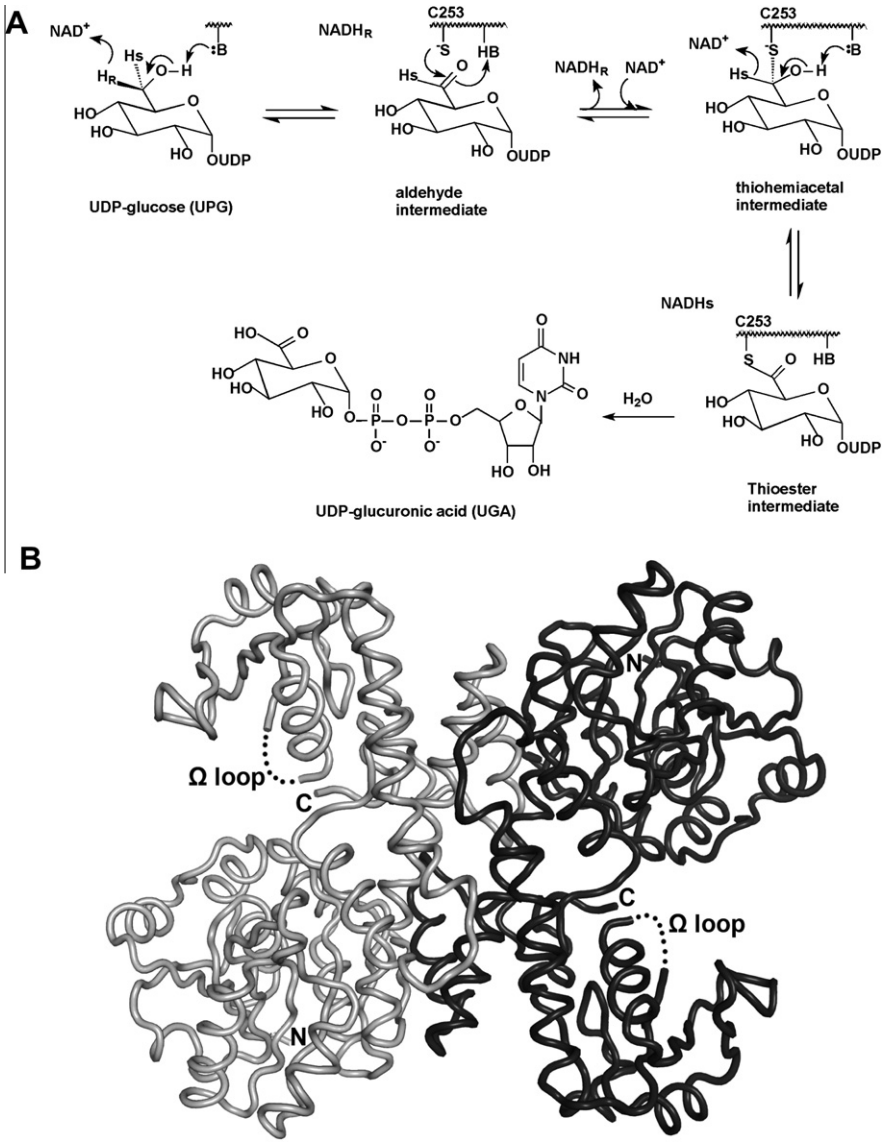

Fig. 1. The reaction mechanism and overall structure of Ugd. (A) Ugd catalyzes two successive NAD^+-dependent oxidation reactions of UPG to yield UGA. The last step, hydrolysis of the covalent UGA-enzyme intermediate is essentially irreversible. (B) A dimer is the basic assembly unit for Ugd. For clarity, the *Kp*Ugd/6His structure is shown with the two subunits in different shades of gray.

PDB code: 2O3 J), Human (*Hs*Ugd; PDB code: 2Q3E, 2QG4, 3ITK and 3KHU) (Lee et al., 2009) have been determined. Structural analyses have also been carried out for the *Sphingomonas* and *Burkholderia* enzymes (Rocha et al., 2010a,b). The oligomeric state of the human and bovine enzymes is a hexamer (Franzen et al., 1981; Lee et al., 2009), or a trimer of dimers, whereas that of *Escherichia coli*, *P. aeruginosa* and *Cryptococcus neoformans* is a dimer (Hung et al., 2007; Schiller et al., 1973; Thompson et al., 1994). Here we present the crystallographic structures of Ugd from a virulent strain of *K. pneumoniae* (*Kp*Ugd) in its apo form, in complex with substrate, substrate and cofactor, and product, as well as a His-tag inhibited form. The structures not only provide new insights into the catalytic mechanism of *Kp*Ugd but also identify K256 and D257 as two critical residues for binding to the second UGA that accounts for a unique regulation mechanism.

2. Materials and methods

2.1. Cloning and protein preparation

The *K. pneumoniae* strain NTUH-K2044 was isolated from patients with septicemia at National Taiwan University Hospital (Wu et al., 2009). The gene fragment of *Kp*Ugd (*ugd*) was provided by Prof. Shih-Feng Tsai. After amplification by polymerase chain reaction, the product encoding *ugd* was digested with *Eco*RI and *Xho*I and cloned into the expression vector pET-28a (Novagen). The *ugd* gene carried by the plasmid was preceded and followed by a six-histidine tag (His_6-tag) coding sequence. Later, site-specific mutagenesis was performed using QuikChange® (Stratagene) to introduce a stop codon before the second His_6-tag sequence to restore the original C-terminus (Table S1). Each construct was transformed into a non-auxotrophic *E. coli* strain BL21 (DE3) competent cell. The proteins were expressed and purified as described previously (Chen et al., 2010). Each batch was grown in LB medium containing 50 μg/L kanamycin to an OD_{600} of ~0.6, and induced with 1.0 mM IPTG (MDBio Inc.) for 18 h at 20 °C. Each overexpressed protein was purified by chromatography using a Ni^{2+}-NTA column (GE Healthcare), which was eluted by a linear gradient of imidazole from 20 to 500 mM. After buffer exchange with a pH 8.7 buffer of 100 mM Tris–HCl (Merck) by FPLC using a HiPrepTM 26/10 desalting column (GE Healthcare), the protein solution was concentrated by using an Amicon centrifugal concentrator with 30 kDa cut-off (Millipore, MA, USA), and stored at −80 °C. The two recombinant proteins, *Kp*Ugd/6His (containing two His_6-tags) and *Kp*Ugd (one His_6-tag), were obtained with higher than 95% purity, estimated using SDS–PAGE.

2.2. Crystallization

The *Kp*Ugd/6His and *Kp*Ugd solutions were adjusted to 3.5 mg/ml in 100 mM Tris–HCl buffer (pH 8.7) containing 20 mM $MgCl_2$ and 2 mM dithiothreitol. The sitting-drop vapor diffusion method was employed, in which 1 μl protein solution was mixed with 1 μl reservoir. The *Kp*Ugd/6His crystals were obtained at 4 °C with a reservoir solution of 0.1 M Tris–HCl buffer (pH 8.0), 0.8 M sodium formate (Fluka) and 14% (w/v) polyethylene glycol (PEG) 8000. Crystallization of *Kp*Ugd/UGA at 10 °C used 20 mM CAPS buffer (pH 11.0, Hampton), 6% (w/v) PEG 8000, and 16% (w/v) ethyleneglycol (Hampton) as a reservoir, where UGA (Sigma) was added to the protein solution with a final concentration of 4 mM. Crystals of *Kp*Ugd/UPG complex were also obtained by cocrystalliztion with 2 mM UPG (Fluka) at 10 °C in a reservoir solution containing 0.1 M Tris–HCl buffer (pH 8.0), 0.8 M sodium formate (Fluka) and 19–25% (w/v) PEG 2000 monomethyl ether (Fluka). The apo-form *Kp*Ugd crystals were prepared as described above for the *Kp*Ugd/UPG complex but it used a different cryoprotectant (250 mM $MgCl_2$, 120 mM NaCl, 23% PEG 3350 and 8% glycerol). The *Kp*Ugd/UPG/NADH crystals were obtained by in-drop soaking of the *Kp*Ugd/UPG crystals for 5 h with identical buffer solution but containing 5 mM NADH.

2.3. Data collection and structural analyses

Crystals were soaked for 5–10 s in a cryoprotectant (the reservoir solution containing 17% ethyleneglycol) before flash-cooling to 100 K in a stream of cold nitrogen. X-ray diffraction data were collected at the SPXF beamline BL13B1 at the National Synchrotron Radiation Research Center (NSRRC), Taiwan, and at beamlines BL-17A and BL-NW12 at the Photon Factory (PF), Japan. The data were processed and scaled by using HKL2000 (Otwinowski and Minor, 1997). The structure of *Kp*Ugd/6His was first determined by the molecular replacement program AMORE (Navaza, 1994) using the structure of *Sp*Ugd (PDB ID: 1DLI) (Campbell et al., 2000) as a search model, and subsequently used in solving the other structures. The apo-form *Kp*Ugd and the complex crystals belong to the same monoclinic space group of C2, except for the *Kp*Ugd/UGA crystal, which belongs to the hexagonal space group $P6_422$. Both crystals contained one Ugd monomer in each asymmetric unit. Model building and refinement were performed with O (Jones et al., 1991), XtalView (McRee, 1999), CNS (Brunger et al., 1998), CCP4 (Collaborative Computational Project, 1994) and Coot (Emsley and Cowtan, 2004). The NADH in the *Kp*Ugd/UPG/NADH complex had clear electron density, but either in this ternary complex or in the binary *Kp*Ugd/UPG complex, the UDP-sugar lacked density for the glucose 1-phosphate moiety and was modeled as a UMP. The *Kp*Ugd/UGA complex had two bound UGA molecules, one in the active site and the other in a different site. All refined models maintained good stereochemistry, as evaluated by PROCHECK (Laskowski et al., 1993). The molecular figures were produced by using PyMOL (Delano, 2002) and UCSF Chimera (Pettersen et al., 2004).

2.4. Enzyme assays

The enzyme activity was determined by measuring the forward reaction rate of UPG oxidation, in which the change in absorbance of the product NADH was monitored at 340 nm (Easley et al., 2007). A typical reaction mixture for *Kp*Ugd contained 50 mM Tris–HCl buffer (pH 8.7), 1 mM dithiothreitol, 0.5 mM NAD^+, and 1 mM UPG. All enzyme assays were carried out at 25 °C in a final volume of 200 μl. Initial velocities were measured during the first 30 s after adding the enzyme to a final concentration of 0.1 nM. Kinetic parameters were obtained by varying the concentration of [NAD^+] varying from 0 to 0.5 mM while keeping [UPG] constant at 1.0 mM, or with [UPG] varying from 0 to 3.0 mM while fixing [NAD^+] at 0.5 mM. Using the program GraphPad, the K_m and V_{max} values for UPG were calculated by fitting the data to the equation $(Y = V_{max}X^h/(X^h + Km^h))$, in which Y, X, and h represent the reaction velocity, the substrate concentration, and the Hill coefficient, respectively. The kinetic constants for NAD^+ were determined by fitting with the formula $Y = V_{max} \times X/(K_m + X)$. All values are the average of triplicate repeats.

Inactivation kinetics was measured under similar conditions as described above. The substrate concentration [UPG] was varied from 0.2 to 1.5 mM with [NAD^+] held constant at 0.5 mM, and the inhibitor concentration [UGA] was also varied from 50 to 400 μM. The kinetic parameters were calculated by nonlinear regression using the program PRISM, in which one best-fit value for the entire set of data was obtained according to the equations $Y = V_{max} \times X/(K_{mObs} + X)$ and $K_{mObs} = K_m \times (1 + [I]/K_i)$, where Y, X, and $[I]$ present the reaction velocity, the substrate concentration,

and the concentration of inhibitor. Protein concentration was determined by the Bradford method (Bradford, 1976), using bovine serum albumin as a standard.

3. Results

3.1. Overall architecture

The monomer of *Kp*Ugd contains 388 amino acids, and it shows significant similarity with those from various other organisms when the sequences are aligned using the program BioEdit (Thompson et al., 1994) (Fig. S2). When compared with *Kp*Ugd, *E. coli* Ugd (Rasko et al., 2008), *S. pneumoniae* Ugd (Bentley et al., 2006), *Sp*Ugd (Campbell et al., 2000), *Pg*Ugd, *Ce*Ugd and *Hs*Ugd (Lee et al., 2009) show overall sequence identities of 99%, 61%, 54%, 28%, 25% and 28%, respectively. A major difference is located in the C-terminus, with approximately 50 additional residues found in *Pg*Ugd, *Ce*Ugd and *Hs*Ugd. The C-terminal extension in the eukaryotic enzymes is responsible for hexamer formation, whereas the prokaryotic enzymes exist mostly as a dimer (Franzen et al., 1981; Hung et al., 2007; Lee et al., 2009; Schiller et al., 1973; Thompson et al., 1994). There are 51 strictly conserved residues (Fig. S2), presumably of functional importance. These include an NAD^+-binding "fingerprint" (residues 7–12 in *Kp*Ugd) in the N-terminal domain with the P-loop motif of GxGxxG (Hung et al., 2007) and a highly conserved active-site signature sequence of GGxCxxKD (Campbell et al., 2000; Lee et al., 2009). Interestingly, the C-terminal domain of *Kp*Ugd contains two candidate regions, A293–V298 (ARKPKV) and M322–A327 (MKRIKA), that match the charged XBBXBX consensus sequence of the heparin sulfate binding site, where B is a basic amino acid and X is hydropathic (neutral and hydrophobic) (Levy-Adam et al., 2005). The XBBXBX consensus sequence can be found in several Ugd from Gram-positive and negative bacteria, but not in those with solved structures.

The crystal structures of *Kp*Ugd reported here include a ligand-free enzyme with a C-terminal His_6-tag (*Kp*Ugd/6His) and the apo-form enzyme (*Kp*Ugd/Apo). The other structures are in complex with (1) the substrate UPG (*Kp*Ugd/UPG), (2) UPG and the cofactor NADH (*Kp*Ugd/UPG/NADH), and (3) the product UGA (*Kp*Ugd/UGA). Some statistics of the data collection and refinement are shown in Table 1. In all crystals the asymmetric unit contains one monomer, but a dimer similar to those of the other known Ugd structures is formed with a crystallographic dyad-related monomer. The extensive interface area of 2600 $Å^2$, calculated by the PISA server (http://pdbe.org/pisa), also suggests the formation of a dimer. Using analytical ultracentrifuge, we further confirmed that *Kp*Ugd exists as a dimer in solution (Fig. S3). Similar to other Ugd structures, the *Kp*Ugd monomer comprises two discrete α/β Rossmann-fold domains connected by a long helix α9 (47 Å, residues 190–221; Fig. 2A). The N-terminal "nucleotide-binding" domain (N domain; residues 1–189) binds to the coenzyme and the C-terminal "catalytic" domain (C domain; residues 222–388) binds to the substrate. Similar to *Sp*Ugd (Campbell et al., 2000), the interdomain pseudo-symmetry also exists in *Kp*Ugd, as reflected by the root-mean-square deviation (RMSD) of about 2.0 Å for more than 40 pairs of Cα atoms in the two domains. The additional C-terminal residues in *Pg*Ugd, *Ce*Ugd and *Hs*Ugd constitute the helix α16 and the strand βQ (Fig. 2B). In the 1.4-Å structure of *Kp*Ugd/6His, the His_6-tag was accommodated within the substrate-binding cavity, stabilized by the interactions with Y242, G250, F385 and D388 (Fig. S4), rather than exposed to the solvent. As a result, *Kp*Ugd/6His was inactivated by the His_6-tag. No activity was detected even after three-hour incubation of the enzyme with substrate and cofactor. As reported previously for *Sp*Ugd (Campbell et al., 2000), the C domain contains an Ω loop, which is not present in the N domain. In our crystals, only the product-bound *Kp*Ugd/UGA showed good electron densities for this loop (304–315). It could not be seen in the other four crystals, probably due to flexibility.

3.2. The coenzyme-binding site

The structure of *Kp*Ugd/Apo, determined at 1.9-Å resolution is essentially identical to that of *Kp*Ugd/6His except for the absence of the C-terminal His_6-tag. The overall protein conformations in the *Kp*Ugd/UPG and *Kp*Ugd/UPG/NADH complex structures at 1.5

Table 1
Data collection and refinement statistics for the crystals of *KpUgd*. Numbers in parentheses are for the highest resolution shells.

	6His	Apo	UPG	UPG/NADH	UGA
Data collection					
X-ray source	PF NW12	PF NW12	PF 17A	NSRRC 13B	NSRRC 13B
Space group	C2	C2	C2	C2	$P6_422$
Unit cell a, b, c (Å)	108.0, 63.7, 79.1	106.9, 63.7, 78.1	106.9, 63.2, 79.2	108.1, 63.6, 78.6	133.4, 133.4, 187.3
α, β, γ (°)	90, 114.7, 90	90, 113.1, 90	90, 114.1, 90	90, 114.2, 90	90, 90,120
Resolution (Å)	30–1.4 (1.45–1.40)	30–1.9 (1.97–1.90)	30–1.5 (1.55–1.50)	30–1.7 (1.76–1.70)	30–2.7 (2.80–2.70)
Number of observations	679935 (48616)	146386 (14460)	394286 (34661)	304732 (29602)	411614 (41162)
Unique reflections	94272 (8420)	37761 (3759)	77013 (7535)	53413 (5286)	27652 (2708)
Completeness (%)	98.2 (86.1)	99.2 (99.7)	99.7 (97.8)	99.7 (99.9)	99.9 (100)
Average I/σ(I)	49.7 (3.0)	25.9 (3.5)	21.7 (3.3)	26.5 (3.4)	35.7 (7.8)
R_{merge} (%)	3.5 (40.3)	5.2 (41.7)	6.1 (36.5)	6.3 (45.6)	8.1 (45.7)
Refinement					
Number of positive reflections	90392 (7209)	36250 (3234)	74004 (6574)	50898 (4578)	26633 (2441)
R_{work} (95% data)	0.169 (0.257)	0.175 (0.242)	0.164 (0.236)	0.165 (0.233)	0.185 (0.262)
R_{free} (5% data)	0.190 (0.283)	0.222 (0.305)	0.190 (0.257)	0.198 (0.234)	0.226 (0.290)
R.m.s.d bond distance (Å)	0.020	0.020	0.020	0.019	0.020
R.m.s.d bond angle (°)	1.8	1.8	1.8	1.9	2.1
Ramachandran plot (% non-Pro non-Gly residues)					
In most favored regions	91.7	92.1	91.8	91.2	88.0
In additional allowed regions	8.0	7.6	7.9	8.5	11.7
In generously allowed regions	0.0	0.0	0.0	0.0	0.0
In disallowed regions	0.3	0.3	0.3	0.3	0.3
Average B ($Å^2$)/Number of non-H atoms					
Protein	19.6/3078	26.2/2994	18.3/2994	16.8/2984	40.1/3076
Water	36.6/751	39.2/472	37.4/664	29.0/428	45.1/158
Ligand			17.8/21	19.8/65	42.7/88

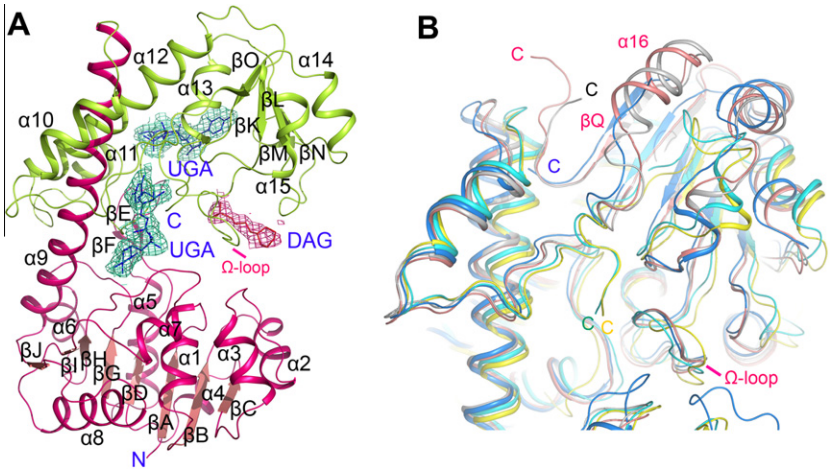

Fig. 2. The monomer of *Kp*Ugd/UGA and structural comparison with other Ugd. (A) The cartoon diagram of *Kp*Ugd/UGA complex shows two distinct domains, which are colored green for the "coenzyme-binding" N domain and hotpink for the "catalytic" C domain. The final $2Fo - Fc$ electron density map at 2.7 Å is contoured at 1.5-σ level for the UGA and CAPS molecules. (B) The Ugd monomers from *K. pneumoniae* (yellow), *S. pyogenes* (PDB code: 1DLJ, cyan), *P. gingivalis* (PDB code: 3GG2, blue), *C. elegans* (PDB code: 2O3J, pink), and human (PDB code: 2QG4, gray) are superimposed. A major structural difference between the eukaryotic Ugd and the bacterial enzymes occurs near the C terminus.

and 1.7-Å resolution are also the same (Fig. S5). The RMSD between these four models range from 0.24 to 0.67 Å for 377 to 379 Cα-atoms, with the largest difference seen in *Kp*Ugd/Apo. Because the cofactor-bound crystals were prepared by soaking, the NAD(H) binding site should be readily accessible. As shown in Fig. 3A (and Fig. S6), the open pocket indeed leaves the NAD(H) molecule exposed to the bulk solvent, except for the nicotinamide moiety, which is partially covered by the Ω loop if it is present. This pocket is similar to those of GDP-4-keto-6-deoxymannose 3,5-epimerase/reductase (Helander et al., 1996) and dTDP-6-deoxy-L-*lyxo*-4-hexulose reductase (Campbell and Tanner, 1999), in which the cofactor could be readily exchanged. The adenine ribose is adjacent to the GxGxxG "fingerprint" of Rossmann fold, located in the βA-α1 turn, whereas the nicotinamide ring is placed in a typical *syn* orientation identical to those *Sp*Ugd and *Hs*Ugd (Campbell et al., 2000; Lee et al., 2009). The coenzyme is held in place by V11,

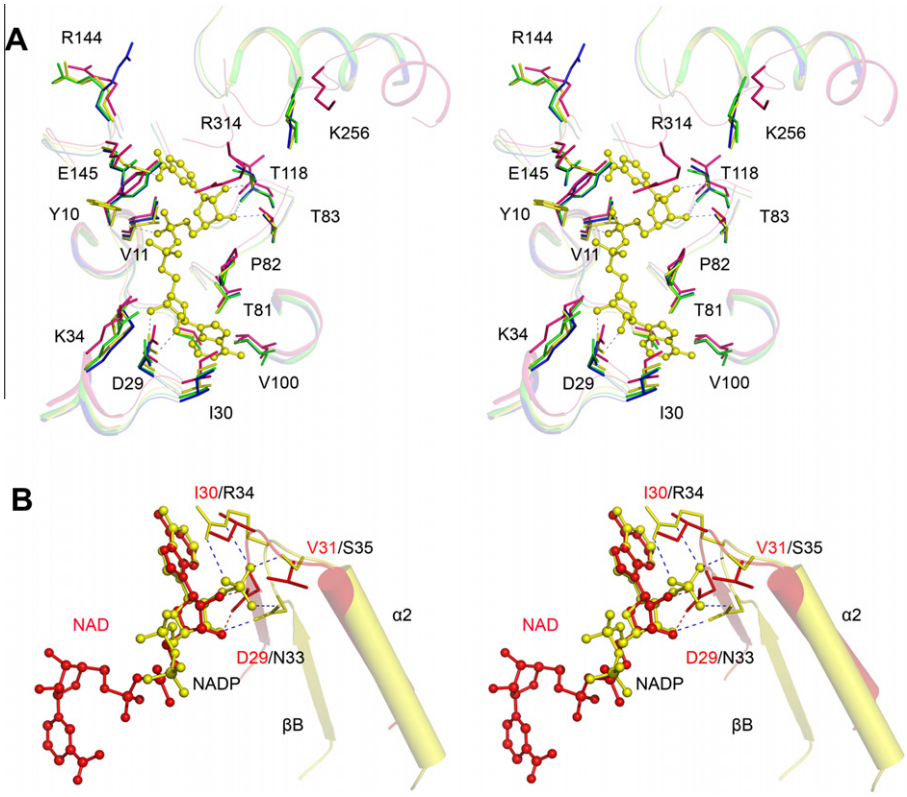

Fig. 3. Stereoviews of the coenzyme-binding site. (A) The surrounding amino-acid residues in the cofactor-binding site of *Kp*Ugd/UPG/NADH are compared by superimposition with the other four *Kp*Ugd structures. NADH and residues from *Kp*Ugd/UPG/NADH complex structure are colored yellow. Those in *Kp*Ugd/UGA, *Kp*Ugd/UPG and *Kp*Ugd/Apo are coloured hotpink, blue and green, respectively. (B) The residues in the N domain that provide the specificity for interactions with NADH (yellow) in *Kp*Ugd and NADPH (red) in *Ec*6PGDH are compared by superimposition. The bound cofactors are represented as ball-and-stick models.

D29, I30, K34, T81, P82, T83, V100, T118, R144 and E145, all from the N domain of the protein (Fig. 3A). Additional interactions may be contributed by the overhanging side chain of R314 from the flexible Ω loop in the C domain. The interactions are similar to those observed in the other Ugd structures (Campbell et al., 2000; Lee et al., 2009). A recent study showed that *E. coli* Ugd is activated by Y71 phosphorylation (Lacour et al., 2008). In the *Kp*Ugd/UPG/NADH structure, the Y71 side chain forms a hydrogen bond with S6 in a cavity adjacent to V100 and it is 5.4 Å from the adenine ring. If Y71 is phosphorylated, the phosphate group can occupy the cavity, exclude solvent molecules, and forms additional hydrogen bonds with the adenine ring of NAD. It may also interact with a nearby K67. These new bonds can increase the enzyme's affinity to the cofactor.

It has been mentioned before that the N domain of *Sp*Ugd is structurally homologous to 6-phosphogluconate dehydrogenase (6PGDH) (Campbell et al., 2000). However, some difference does exist. In 6PGDH, the nicotinamide ring of the reduced cofactor is rotated about its N-glycosidic bond by about 180° during catalysis, placing the ring into a position previously occupied by substrate (Chen et al., 2010). In contrast, superposition of the oxidized and reduced cofactors from the Ugd structures shows nearly identical orientation of the nicotinamide ring (Fig. S7). The nicotinamide moiety of the NAD(H) bound to *Kp*Ugd is positioned by a strictly conserved E145 that may prevent ring flipping, whereas the smaller residue S128 in 6PGDH provides more space for ring flipping (Chen et al., 2010). The tighter binding of the nicotinamide in Ugd than in 6PGDH suggests that the oxidation reaction catalyzed by Ugd does not require ring flipping. Furthermore, the ability to discriminate between 2'-hydroxyl of NAD^+ and the 2′-phosphate of $NADP^+$ also depends on the properties of the amino acid residues lining the pockets. In the *E. coli* 6PGDH complex with 6-phosphogluconate and $NADP^+$ (Chen et al., 2010), three residues N33, R34 and S35 in the loop between strand βB and helix α2 favor interactions with the 2'-phosphate of $NADP^+$ (Fig. 3B). The positively charged guanidinium group of R34 attracts the negatively charged 2′-phosphate of $NADP^+$. However, the three residues are replaced by D29, I30 and V31 in the corresponding loop of *Kp*Ugd. D29 forms direct hydrogen bonds with the 2′ and 3′-OH of NAD(H) and, along with V31, occupies the space for the 2′-phosphate of $NADP^+$. The negatively charged D29 also actively repel the negatively charged 2′-phosphate of $NADP^+$. By exerting steric hindrance and electronstatic repulsion, the conserved acidic amino acid D29 is essential for the specific binding of NAD^+ to *Kp*Ugd.

3.3. The substrate-binding site

Although both of the *Kp*Ugd/UPG and *Kp*Ugd/UPG/NADH crystals were obtained by co-crystallization, only a UMP was seen in the difference Fourier maps (at 1.5 and 1.7 Å). The absence of glucose 1-phosphate moiety could be a result of disorder in the crystal or partial hydrolysis during crystallization. In either case, the data indicate that the sugar phosphate moiety was not strongly bound to the *Kp*Ugd conformation in the C2 unit cell. The remaining UMP moiety occupies essentially the same position as that in the UDP-xylose complex structure of *Sp*Ugd (Campbell et al., 2000). The protein interacts with the UMP mainly via Y242, N244, S246 and G250 from the C domain, in a stretch of coil between helices α10 and α11. Besides, the *Kp*Ugd/UPG complex also shows a salt bridge between the phosphate group and R144, which is from the N domain (Fig. S7). Despite the lower resolution of 2.7 Å, the *Kp*Ugd/UGA complex structure shows an intact UGA molecule bound to the active site. The mode of UMP-binding is largely identical to that in the C2 crystal, and so is the disposition of the glucuronic acid 1-phosphate moiety to that in the *Sp*Ugd/UGA/NAD^+ complex (Campbell et al., 2000). The major interactions are provided by F142, L143 and E145 form the N domain and K197 and N201 from the inter-domain helix α9 (Fig. 4A). The side chain of K307 in the Ω loop is 4.8 Å from the pyrophosphate group. Additional hydrogen bonds are observed between the C-terminal carboxylate of D388 and the 2′ and 3′-OH groups of the ribose, and between the side chain of R237 from the other subunit in the dimer and the 2'' and 3''-OH groups of the glucuronic acid.

The Ω loop in the *Kp*Ugd/UGA complex does not interact directly with the bound UGA molecule. The reason that it could be seen in the $P6_422$ crystal, but not in the C2 crystals, may lie in the two stabilizing hydrogen bonds from E145 to S310 and D311 (Fig. 4A). E145 is conserved among all known structures (Fig. S2), and so is the length of the Ω loop. Mutation of E145Q in *Sp*Ugd showed that it is not catalytically important (Ge et al., 2004). The *Kp*Ugd/UGA structure presented here suggests that a glutamine can still interact very well with the Ω loop. When compared with those in the apo enzyme and the other complex structures, the βH-α7 loop, which contains E145, is shifted toward the bound product (Fig. S8). In fact, the entire N domain is moved closer to the active-site pocket in the hexagonal *Kp*Ugd crystal, resulting in an overall "closed" conformation which is more akin to that in the *Sp*Ugd crystals (Campbell et al., 2000), with an overall RMSD of 0.84 Å between 324 Cα pairs (matching distance = 2.0 Å). Eight residues (307–314) in the Ω loop show more than 2 Å deviations. By comparison, the monoclinic *Kp*Ugd structures have an "open" conformation. The two protein conformations differ by an approximately 14° rotation of the N domain, or a rigid-body movement with a largest shift of 17 Å in the protein backbone. By this movement, the two domains in the four monoclinic *Kp*Ugd crystals can be superimposed separately on those in the hexagonal crystal by RMSD of 0.34–0.43 Å (N) and 0.64–0.80 Å (C) for 183–184 and 105–131 Cα pairs, respectively. The monoclinic N and C domains of *Kp*Ugd can also be superimposed with those of *Sp*Ugd by RMSD of 0.70–0.77 Å and 0.63–0.81 Å for 173–177 and 143–147 Cα pairs (Table S2). Despite the presence of Ω loop and the similar overall disposition, the *Kp*Ugd/UGA complex structure (in the $P6_422$ crystal) shows more differences from *Sp*Ugd, particularly in the C domain, than do the other *Kp*Ugd structures (in C2). In the N domain only the region 86–90 shows some difference.

The sulfur atom of C253 is 6.6 Å from the C6'' of the bound UGA in the hexagonal crystal structure, too far for nucleophilic attack. It is a result of structural changes in the region 250–275, which will be discussed shortly. By domain superposition, if the UGA is placed in the C domain of the *Kp*Ugd/UPG/NADH complex, the C6'' of UGA will lie adjacent to the sulfur atom of C253, with a distance of 2.9 Å, but it will be too far (5.7 Å) from the C4 N atom of NAD(H), the hydride carrier. Nevertheless, if the NAD(H) is fitted into the N domain of *Kp*Ugd/UGA complex, the C6''-C4N distance will be 3.3 Å and the carboxylate group will be parallel to the ring, ready for the reaction (Fig. S9). The side chain of R314 will be 5.9 Å from the pyrophosphate of NAD(H), but it actually interacts with a bound solvent CAPS molecule (Fig. 4B). In the *Sp*Ugd structure a similar arrangement is seen (Campbell et al., 2000), that involves a sulfate ion. If K307 and R314 bind directly to the pyrophosphate groups of UPG and NAD, the Ω loop would move closer to the active site, accompanied by exclusion of solvent molecules. These observations support the open-close conformational switch between the monoclinic and hexagonal crystal structures. The open conformation failed to stabilize the glucose 1-phosphate moiety of UPG, but it allowed the substrate to be washed away with a salt-containing solution and the structure of unbound *Kp*Ugd/Apo to be determined. The disordered Ω loop, previously suggested to act as a mobile "gate" in *Sp*Ugd (Campbell et al., 2000), is also consistent with the mechanism of twofold oxidation that requires rapid exchange of the spent cofactor for a fresh one.

3.4. The allosteric binding site for UGA

In addition to the Ω loop, the C domain of *Kp*Ugd/UGA complex structure also differs from the other *Kp*Ugd (and *Sp*Ugd) structures by a large conformational change in the region of 250–275, beginning with the GGxCxxKD motif near the N-terminus of helix α11 and extending toward helix α12. Regardless of the lower resolution (2.7 Å) of the diffraction data, the extensive structural difference was unambiguously observed in the clear electron density map for this region (Fig. S10). Adjacent to this altered region, a second molecule of UGA, in addition to the one in the active site, is bound to a surface "allosteric" pocket of the enzyme. The pocket is lined with several positively charged residues including K256, K259, K284, K323, R324 and K326 (Fig. S11). The uracil base of the UGA is held in position not only by a hydrogen bond to the K326 side chain but also by stacking interaction with the aromatic ring of F345, which moves about 4 Å toward the base plane when compared with that in the other structures (Fig. S11). The negative charges on the pyrophosphate and the C6''-carboxylate groups are compensated by direct bonding to K256, K284 and R324, as

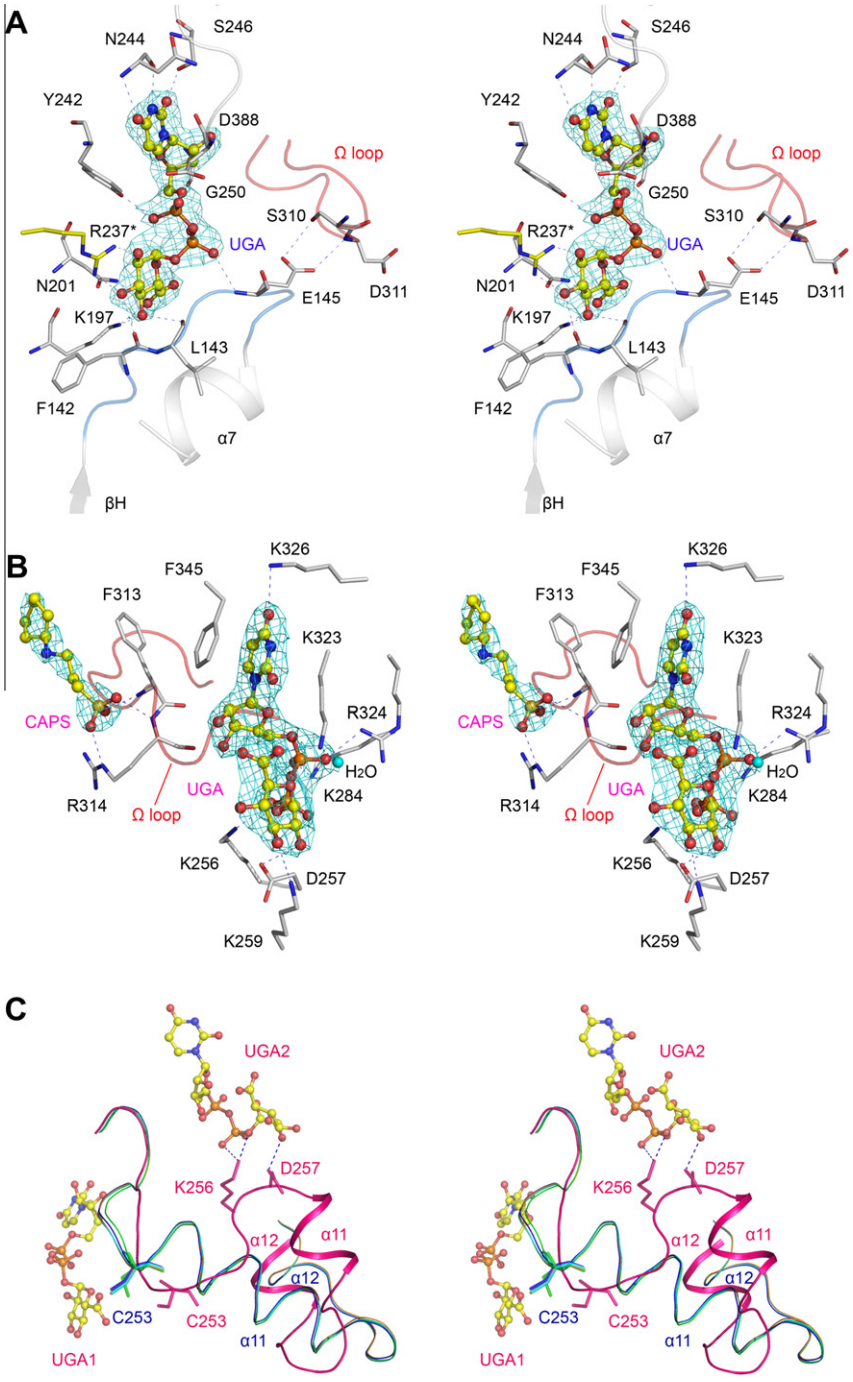

Fig. 4. Stereoviews of the *Kp*Ugd-UGA interactions. (A) In the active site, the bound product UGA is shown as a ball-and-stick model. The surrounding residues are shown as stick models. A refined 2*Fo*−*Fc* electron density map is contoured at 1.5-σ level and shown as cyan mesh. The residue R237 from the other subunit, which binds to the UGA, is highlighted in yellow, and so is the Ω loop in pink. (B) In the allosteric binding site, a network of hydrogen bonds holds the second UGA molecule, which is shown along with a CAPS molecule and the corresponding 2*Fo*−*Fc* electron densities at 1.3-σ level (cyan mesh). (C) Conformational changes are observed in *Kp*Ugd/UGA complex (hotpink) that the position of the α11 is different from those in *Kp*Ugd/Apo (blue), *Kp*Ugd/6His (green), *Kp*Ugd/UPG (cyan), and *Kp*Ugd/UPG/NADH (orange). All models are superimposed by their catalytic domains. The movements of C253, K256 and D257 lead to an inactive enzyme structure of *Kp*Ugd/UGA.

well as a water-mediated interaction with K323 (Fig. 4B). In addition, the side chains of D257 and K259 make two hydrogen bonds to the 3'' and 4''-OH of the glucuronic acid moiety.

Surface charge distribution analysis using the APBS protocol (Baker et al., 2001) indicates that the second UGA-binding pocket is pre-existing among all *Kp*Ugd structures (Fig. S12). Here the motif of MKRIKA (322–327) is brought into light, representing a novel formation of a surface pocket enriched with basic amino acids, most prominently in the *Kp*Ugd/UGA structure. This motif matches the above mentioned XBBXBX consensus sequence comprising basic side chains for binding to highly negatively charged oligosaccharides on cell surface (Levy-Adam et al., 2005). Although *Kp*Ugd exists in the cytosol, the MKRIKA motif, along with K256, K259 and K284, forms a positively charged surface patch on *Kp*Ugd that not only provides significant electrostatic environment to balance the negatively charged phosphate groups of the second UGA molecule, a similar feature as for heparin sulfate binding, but also involves a number of specific interactions that eventually lead to structural alteration in the active site. Sequence alignment shows that K256, D257, K259 and K284 are largely conserved, whereas only one basic residue is found in the XBBXBX region of *Sp*Ugd, *Pg*Ugd, *Ce*Ugd and *Hs*Ugd (Fig. S2). This is consistent with the observation that the second UGA-binding site is present only in *Kp*Ugd but not in the other Ugd structures (Fig. S12). Furthermore, an insertion in the eukaryotic *Pg*Ugd, *Ce*Ugd and *Hs*Ugd, located between the equivalent strands to βL and βM in *Kp*Ugd, forms an α-helix that occludes the space where the second UGA molecule would bind (Fig. S13).

The *Kp*Ugd/UGA crystals were obtained by co-crystallization with UGA. Consequently, the conformational change should have occurred in the protein prior to crystallization, most likely as a result of binding to the second UGA molecule. Because the allosteric UGA binding involves K256, D257 and K259, the nearly four-turn helix α11 that contains these residues becomes less than two-turn. The helix is rotated sideways by about 45° and withdrawn from the active site, accompanied by structural rearrangement in its connecting loops (Fig. 4C). The largest shift in Cα position (10 Å) is seen in D257, and even larger shifts (14 Å) are seen in the side chains of Y252 and Y265 (Fig. S14). In the other *Kp*Ugd structures the side chain of Y252 is directed outward the solvent, but in *Kp*Ugd/UGA it moves inward and displaces the original position of L254. The two proceeding glycine residues apparently provide flexibility for this movement. The conformational change carries C253, K256 and D257 away from the active site and these residues, as mentioned above for C253, become unable to react with the substrate molecule. The structural rearrangement propagates through the entire α11-α12 loop. In addition, the region 86–90 of the βE-βF loop (in N domain), which lies adjacent to the altered α11-α12 loop, also shows conformational change as a result of the UGA binding, and the Ω loop of *Kp*Ugd/UGA does not associate with the GGxCxxKD motif as it does in *Sp*Ugd. Taken together, this double UGA-bound structure probably represents an inactive conformation of the enzyme.

3.5. Kinetic and inhibition characteristics

Previous studies suggested a bi-uni-uni-bi Ping-Pong mechanism for the Ugd-catalyzed reaction (Campbell et al., 1997). In addition to *Sp*Ugd (Campbell et al., 2000), other Ugd from *P. aeruginosa* (Hung et al., 2007) and *B. cenocepacia* (Loutet et al., 2009)

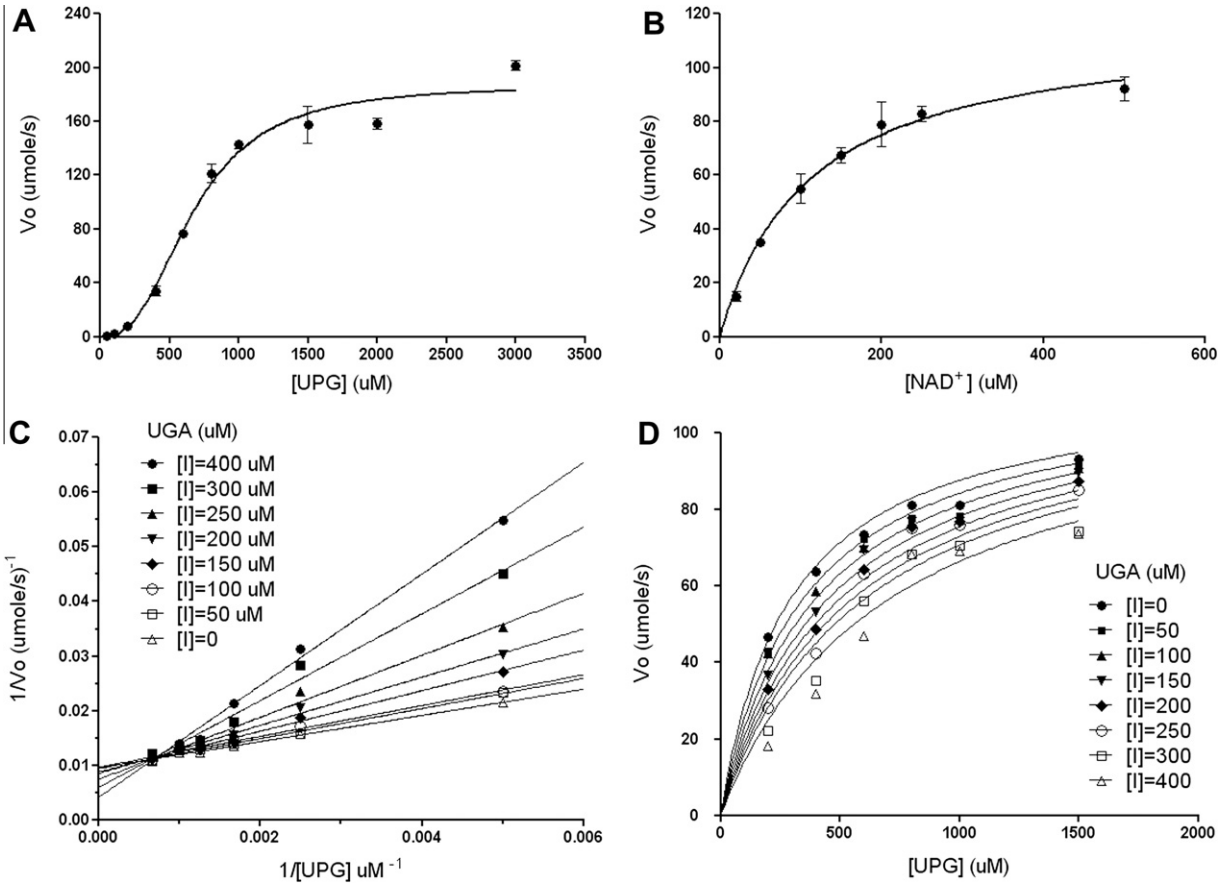

Fig. 5. Basic kinetic properties of *Kp*Ugd. Initial velocity pattern with UPG as the variable substrate is shown in (A) and the pattern with NAD^+ as the variable substrate is shown in (B). Double reciprocal plots of the initial rate data for *Kp*Ugd reveal a competitive inhibition pattern for product with UPG as the variable substrate (C). The pattern of initial velocity in the inhibition studies shows direct curves for substrate saturation (D). The solid lines represent the best fit with single-site binding.

Table 2
Comparison of the kinetic parameters of *K. pneumoniae* and human Ugd.

	V_{max} (nmol min^{-1} mg^{-1})	km-UPG (juM)	k_m-NAD+(μM)
KpUgd	609 ± 58	674 ± 26	110 ± 11
HsUgd[a]	690 ± 9	9.2 ± 0.7	420 ± 27

[a] Published values for *Hs*Ugd from reference (Easley et al., 2007).

have been noted for weak cooperative binding effects of the substrate. For comparison, the overall activity and kinetic parameters of *Kp*Ugd were measured here. Under saturating conditions, the specific activity (V_{max}) of *Kp*Ugd was determined to be 609 ± 58 nmole·mg^{-1}·min^{-1}, which is similar to that of *Hs*Ugd (690 ± 9) (Easley et al., 2007). The results of activity measurement by varying UPG and NAD^+ concentrations are shown in Fig. 5A and B. Interestingly, the velocity dependence on substrate concentration is sigmoidal for UPG, while it is hyperbolic for NAD^+. By fitting the UPG data points with a cooperative binding curve, a Hill coefficient of 2.6 is obtained, indicating strong positive cooperativity for UPG binding to *Kp*Ugd, especially when it is compared with those for the other enzymes (all smaller than 1.67) (Campbell et al., 2000) (Hung et al., 2007) (Loutet et al., 2009). The K_m values of *Kp*Ugd and *Hs*Ugd (Easley et al., 2007) for the substrate and cofactor are compared in Table 2. *Kp*Ugd has a similar binding affinity for NAD^+ but a lower affinity for UPG than that of *Hs*Ugd (Easley et al., 2007), likely owing to the product inhibition caused by UGA. Because UGA was previously found to be a competitive inhibitor of *Sp*Ugd (Campbell et al., 1997), product inhibition analysis was carried out to investigate the effect of UGA on *Kp*Ugd's activity. The double reciprocal plot in Fig. 5C shows a trend for competitive inhibition. Furthermore, the product inhibition measurements yielded a K_i value of 283 μM (Fig. 5D), which is comparable to that for *Sp*Ugd (K_i = 200 μM) (Campbell et al., 1997).

The observation of a sigmoidal curve in the velocity measurement by varying UPG concentration (Fig. 5A) implies that the binding of UPG to *Kp*Ugd does not follow conventional Michaelis–Menten kinetics. Although the double reciprocal plot suggests competitive inhibition (Fig. 5C), the V_{max} was actually reduced by the increasing product concentration (Fig. 5D). Since the chemical structures of UPG and UGA are very similar, both can bind to the allosteric site. The effect of allosteric UPG binding on the enzyme conformation remains to be further investigated.

4. Discussion

The open conformation of *Kp*Ugd in the monoclinic crystals allows us to see how the substrate and cofactor enter and leave the active site. The flexible Ω loop, which serves as a gate to the active site, was not visible in this crystal form. The open conformation should facilitate rapid exchange of the cofactor as well as substrate binding and product release. In fact, the *Kp*Ugd/apo and *Kp*Ugd/UPG/NADH crystals were obtained by washing away the enzyme-bound substrate with a salt-containing cryoprotectant solution and by soaking with a NADH-containing buffer solution. For its catalytic reaction to proceed, the enzyme has to undergo open-close conformational changes by moving the N and C domains, which provide the major interactions for binding to the coenzyme and substrate molecules. In this way the C4N atom of NAD^+ is properly placed at a reactive distance from the C6" atom of UPG. Interestingly, the closed conformation of *Kp*Ugd/UGA observed in the hexagonal crystal, although similar to that of *Sp*Ugd in terms of the domain dispositions (Campbell et al., 2000), turns out to be inactive. Binding of the second UGA to the allosteric surface pocket triggered large structural changes in the region of 250–275, that drag the catalytically important residues C253, K256 and D257 away from the active site. The Ω loop seems to be stabilized in a conformation slightly different from that of a really closed "gate" (Campbell et al., 2000), and the UGA trapped in the active site further prevents the substrate UPG from entering.

Whether UPG also binds to the allosteric site is unclear, but the kinetic analysis shows a Hill coefficient of 2.6, indicating cooperative substrate binding to more than one site. These observations prompt us to propose a mechanism of regulation (Fig. S15). Under conditions where there is more substrate than product, the conversion of UPG to UGA proceeds with the twofold oxidation that uses two equivalents of NAD^+. When the UGA concentration is increased, the product not only competes with the substrate for binding to the active site, but it also occupies the allosteric binding site and inactivates the enzyme by triggering conformational changes. Only after most of the UGA molecules are consumed, for example, by downstream reactions can the enzyme return to its active form. Because the product hydrolysis step is essentially irreversible, stringent *in vivo* control of the reaction catalyzed by Ugd allows the cytoplasmic pools of UPG and UGA to be maintained at an optimal level. Furthermore, since the L-Ara4N biosynthetic pathway begins with the production of UGA by Ugd (Fig. S1), regulating the Ugd activity also controls the biosynthesis of L-Ara4N (Lacour et al., 2008).

The importance of K256 and D257 has been elucidated by mutagenic analysis of the equivalent residues in the human enzyme (Easley et al., 2007; Sommer et al., 2004). In the catalytic mechanism (see Fig. 1), a base has to subtract a proton from the 6"-OH group of UPG. K256 is thought to provide electrostatic interactions with D257, which in turn activates a water molecule that mediates indirect links to the 6"-OH group (Campbell et al., 2000; Sommer et al., 2004). Other basic residues in the active site are supposed to engage mostly in substrate binding. R144 in *Kp*Ugd/UPG binds to the phosphate group of the UMP model, but it is associated with D151 in the other structures. The side chain of K307, visible only in *Kp*Ugd/UGA, can also interact with the pyrophosphate of UGA. Unlike the flexible R144 and K307 that can bind to the phosphate groups, R237 from the other subunit is stationary and interacts with the ribose moiety of the substrate. In addition, the NZ atom of K197 in the *Kp*Ugd/UGA complex, which is equivalent to K204 in *Sp*Ugd (Campbell et al., 2000) and conserved in the Ugd from all other species, is co-planar with the 6"-carboxylate group of UGA and forms a short hydrogen bond of 2.5 Å to it. When the UGA is placed into the C domain of the other *Kp*Ugd structures, the sulfur atom of C253 will also be co-planar with this carboxylate group but on the opposite side with respect to K197. It has been suggested that all intermediates between UPG and UGA are continuously covalently bonded to the enzyme (Campbell et al., 2000; Ge et al., 1998; Ordman and Kirkwood, 1977a; Ridley and Kirkwood, 1973). Judging by the reasonable geometry, in addition to serving directly as a catalytic base, this lysine residue is a good candidate to form a Schiff base with the aldehyde intermediate.

Although the catalytic mechanism is conserved and the turnover rate is about the same for all Ugd from different species, the *K. pneunomiae* enzyme shows an especially low affinity for the substrate, and it also binds to a second UGA at a different site. That UGA is both a competitive inhibitor and an allosteric regulator makes it a good lead compound in the design of inhibitors. Furthermore, the additional residues in the C-terminal region of other (eukaryotic) Ugd prevent UGA from binding to a similar allosteric site, and they are also responsible for the formation of higher oligomers (hexamers for the human enzyme) (Egger et al., 2010). The unexpected observation that the C-terminal His_6-tag occupies the substrate-binding site with a number of well defined hydrogen-bonding interactions also encourages the development of peptide inhibitors (both D and L-forms).

5. PDB deposition

The atomic coordinates and structure factors have been deposited in the Worldwide Protein Data Bank (http://www.wwPDB.org) with wwPDB ID codes of 3PID, 3PHL, 3PLN, 3PLR and 3PJG, respectively, for the *Kp*Ugd/6His, *Kp*Ugd/Apo, *Kp*Ugd/UPG, *Kp*Ugd/UPG/NADH and *Kp*Ugd/UGA crystals.

Acknowledgments

We thank Dr. Wen-Yih Jeng, Dr. Cheng-Chung Lee and Ms. Hui-Ling Shr for technical assistance, the Core Facility for Protein Production and X-ray Structural Analysis (Academia Sinica) for crystallization screening, and the National Synchrotron Radiation Research Center (Taiwan) and Photon Factory (Japan) for beamtime allocations. This work was supported by Academia Sinica and grant NSC97-3112-B-001-017 to A.H.-J.W.

Appendix A. Supplementary data

Supplementary data associated with this article can be found, in the online version, at doi:10.1016/j.jsb.2011.04.010.

References

Baker, N.A., Sept, D., Joseph, S., Holst, M.J., McCammon, J.A., 2001. Electrostatics of nanosystems: application to microtubules and the ribosome. Proc. Natl. Acad. Sci. USA 98, 10037–10041.

Bentley, S.D., Aanensen, D.M., Mavroidi, A., Saunders, D., Rabbinowitsch, E., Collins, M., Donohoe, K., Harris, D., Murphy, L., Quail, M.A., Samuel, G., Skovsted, I.C., Kaltoft, M.S., Barrell, B., Reeves, P.R., Parkhill, J., Spratt, B.G., 2006. Genetic analysis of the capsular biosynthetic locus from all 90 pneumococcal serotypes. PLoS Genet. 2, e31.

Bradford, M.M., 1976. A rapid and sensitive method for the quantitation of microgram quantities of protein utilizing the principle of protein-dye binding. Anal. Biochem. 72, 248–254.

Breazeale, S.D., Ribeiro, A.A., McClerren, A.L., Raetz, C.R., 2005. A formyltransferase required for polymyxin resistance in *Escherichia coli* and the modification of lipid A with 4-Amino-4-deoxy-L-arabinose. Identification and function of UDP-4-deoxy-4-formamido-L- arabinose. J. Biol. Chem. 280, 14154–14167.

Brunger, A.T., Adams, P.D., Clore, G.M., DeLano, W.L., Gros, P., Grosse-Kunstleve, R.W., Jiang, J.S., Kuszewski, J., Nilges, M., Pannu, N.S., Read, R.J., Rice, L.M., Simonson, T., Warren, G.L., 1998. Crystallography and NMR system: a new software suite for macromolecular structure determination. Acta Crystallogr. D Biol. Crystallogr. 54, 905–921.

Burtnick, M.N., Woods, D.E., 1999. Isolation of polymyxin B-susceptible mutants of *Burkholderia pseudomallei* and molecular characterization of genetic loci involved in polymyxin B resistance. Antimicrob. Agents Chemother. 43, 2648–2656.

Campbell, R.E., Tanner, M.E., 1997. Uridine diphospho-alpha-D-gluco-hexodialdose: synthesis and kinetic competence in the reaction catalyzed by UDP-glucose dehydrogenase. Angewandte Chemie-International Edition in English 36, 1520–1522.

Campbell, R.E., Tanner, M.E., 1999. UDP-glucose analogues as inhibitors and mechanistic probes of UDP-glucose dehydrogenase. J. Org. Chem. 64, 9487–9492.

Campbell, R.E., Sala, R.F., van de Rijn, I., Tanner, M.E., 1997. Properties and kinetic analysis of UDP-glucose dehydrogenase from group A streptococci. Irreversible inhibition by UDP-chloroacetol. J. Biol. Chem. 272, 3416–3422.

Campbell, R.E., Mosimann, S.C., van De Rijn, I., Tanner, M.E., Strynadka, N.C., 2000. The first structure of UDP-glucose dehydrogenase reveals the catalytic residues necessary for the two-fold oxidation. Biochemistry 39, 7012–7023.

Chen, Y.Y., Ko, T.P., Chen, W.H., Lo, L.P., Lin, C.H., Wang, A.H., 2010. Conformational changes associated with cofactor/substrate binding of 6-phosphogluconate dehydrogenase from *Escherichia coli* and *Klebsiella pneumoniae*: implications for enzyme mechanism. J. Struct. Biol. 169, 25–35.

Cheng, H.Y., Chen, Y.F., Peng, H.L., 2010. Molecular characterization of the PhoPQ-PmrD-PmrAB mediated pathway regulating polymyxin B resistance in *Klebsiella pneumoniae* CG43. J. Biomed. Sci. 17, 60.

Collaborative Computational Project, N., 1994. The CCP4 suite: programs for protein crystallography. Acta Crystallogr. D Biol. Crystallogr. 50, 760–763.

Dalessandro, G., Northcote, D.H., 1977. Changes in enzymic activities of nucleoside diphosphate sugar interconversions during differentiation of cambium to xylem in sycamore and poplar. Biochem. J. 162, 267–279.

Delano, W.L. 2002. DeLano Scientific, San Carlos, CA, USA, http://www.pymol.org.

Easley, K.E., Sommer, B.J., Boanca, G., Barycki, J.J., Simpson, M.A., 2007. Characterization of human UDP-glucose dehydrogenase reveals critical catalytic roles for lysine 220 and aspartate 280. Biochemistry 46, 369–378.

Egger, S., Chaikuad, A., Kavanagh, K.L., Oppermann, U., Nidetzky, B., 2010. UDP-glucose dehydrogenase: structure and function of a potential drug target. Biochem. Soc. Trans. 38, 1378–1385.

Emsley, P., Cowtan, K., 2004. Coot: model-building tools for molecular graphics. Acta Crystallogr. D Biol. Crystallogr. 60, 2126–2132.

Fang, C.T., Chuang, Y.P., Shun, C.T., Chang, S.C., Wang, J.T., 2004. A novel virulence gene in *Klebsiella pneumoniae* strains causing primary liver abscess and septic metastatic complications. J. Exp. Med. 199, 697–705.

Franzen, B., Carrubba, C., Feingold, D.S., Ashcom, J., Franzen, J.S., 1981. Amino acid sequence of the tryptic peptide containing the catalytic-site thiol group of bovine liver uridine diphosphate glucose dehydrogenase. Biochem. J. 199, 599–602.

Gatzeva-Topalova, P.Z., May, A.P., Sousa, M.C., 2005. Structure and mechanism of ArnA: conformational change implies ordered dehydrogenase mechanism in key enzyme for polymyxin resistance. Structure 13, 929–942.

Ge, X., Campbell, R.E., van de Rijn, I., Tanner, M.E., 1998. Covalent adduct formation with a mutated enzyme: Evidence for a thioester intermediate in the reaction catalyzed by UDP-glucose dehydrogenase. J. Am. Chem. Soc. 120, 6613–6614.

Ge, X., Penney, L.C., van de Rijn, I., Tanner, M.E., 2004. Active site residues and mechanism of UDP-glucose dehydrogenase. Eur. J. Biochem. 271, 14–22.

Guo, L., Lim, K.B., Gunn, J.S., Bainbridge, B., Darveau, R.P., Hackett, M., Miller, S.I., 1997. Regulation of lipid A modifications by *Salmonella typhimurium* virulence genes phoP-phoQ. Science 276, 250–253.

Helander, I.M., Kato, Y., Kilpelainen, I., Kostiainen, R., Lindner, B., Nummila, K., Sugiyama, T., Yokochi, T., 1996. Characterization of lipopolysaccharides of polymyxin-resistant and polymyxin-sensitive *Klebsiella pneumoniae* O3. Eur. J. Biochem. 237, 272–278.

Huh, J.W., Yoon, H.Y., Lee, H.J., Choi, W.B., Yang, S.J., Cho, S.W., 2004. Importance of Gly-13 for the coenzyme binding of human UDP-glucose dehydrogenase. J. Biol. Chem. 279, 37491–37498.

Hung, R.J., Chien, H.S., Lin, R.Z., Lin, C.T., Vatsyayan, J., Peng, H.L., Chang, H.Y., 2007. Comparative analysis of two UDP-glucose dehydrogenases in *Pseudomonas aeruginosa* PAO1. J. Biol. Chem. 282, 17738–17748.

Jiang, S.S., Lin, T.Y., Wang, W.B., Liu, M.C., Hsueh, P.R., Liaw, S.J., 2010. Characterization of UDP-glucose dehydrogenase and UDP-glucose pyrophosphorylase mutants of *Proteus mirabilis*: defectiveness in polymyxin B resistance, swarming, and virulence. Antimicrob. Agents Chemother. 54, 2000–2009.

Jones, T.A., Zou, J.Y., Cowan, S.W., Kjeldgaard, M., 1991. Improved methods for building protein models in electron density maps and the location of errors in these models. Acta Crystallogr. A 47 (Pt 2), 110–119.

Lacour, S., Bechet, E., Cozzone, A.J., Mijakovic, I., Grangeasse, C., 2008. Tyrosine phosphorylation of the UDP-glucose dehydrogenase of *Escherichia coli* is at the crossroads of colanic acid synthesis and polymyxin resistance. PLoS ONE 3, e3053.

Laskowski, R.A., MacArthur, M.W., Moss, D.S., Thornton, J.M., 1993. PROCHECK: a program to check the stereochemical quality of protein structures. J.Appl. Cryst. 26, 283–291.

Lee, H.S., Son, Y.J., Chong, S.H., Bae, J.Y., Leem, C.H., Jang, Y.J., Choe, H., 2009. Computational analysis of the quaternary structural changes induced by point mutations in human UDP-glucose dehydrogenase. Arch. Biochem. Biophys. 486, 35–43.

Levy-Adam, F., Abboud-Jarrous, G., Guerrini, M., Beccati, D., Vlodavsky, I., Ilan, N., 2005. Identification and characterization of heparin/heparan sulfate binding domains of the endoglycosidase heparanase. J. Biol. Chem. 280, 20457–20466.

Loutet, S.A., Bartholdson, S.J., Govan, J.R., Campopiano, D.J., Valvano, M.A., 2009. Contributions of two UDP-glucose dehydrogenases to viability and polymyxin B resistance of *Burkholderia cenocepacia*. Microbiology 155, 2029–2039.

McRee, D.E., 1999. XtalView/Xfit–A versatile program for manipulating atomic coordinates and electron density. J. Struct. Biol. 125, 156–165.

Navaza, J., 1994. AMoRe: an automated package for molecular replacement. Acta Crystallogra. A 50, 157–163.

Ordman, A.B., Kirkwood, S., 1977a. Mechanism of action of uridine diphoglucose dehydrogenase. Evidence for an essential lysine residue at the active site. J. Biol. Chem. 252, 1320–1326.

Ordman, A.B., Kirkwood, S., 1977b. UDPglucose dehydrogenase. Kinetics and their mechanistic implications. Biochim. Biochim. Biophys. Acta 481, 25–32.

Otwinowski, Z., Minor, W., 1997. Processing of X-ray diffraction data collected in oscillation mode. Methods Enzymol. 276, 307–326.

Pettersen, E.F., Goddard, T.D., Huang, C.C., Couch, G.S., Greenblatt, D.M., Meng, E.C., Ferrin, T.E., 2004. UCSF Chimera–a visualization system for exploratory research and analysis. J. Comput. Chem. 25, 1605–1612.

Podschun, R., Ullmann, U., 1998. *Klebsiella spp.* as nosocomial pathogens: epidemiology, taxonomy, typing methods, and pathogenicity factors. Clin. Microbiol. Rev. 11, 589–603.

Princivalle, M., de Agostini, A., 2002. Developmental roles of heparan sulfate proteoglycans: a comparative review in *Drosophila*, mouse and human. Int. J. Dev. Biol. 46, 267–278.

Rasko, D.A., Rosovitz, M.J., Myers, G.S., Mongodin, E.F., Fricke, W.F., Gajer, P., Crabtree, J., Sebaihia, M., Thomson, N.R., Chaudhuri, R., Henderson, I.R., Sperandio, V., Ravel, J., 2008. The pangenome structure of *Escherichia coli*: comparative genomic analysis of *E. coli* commensal and pathogenic isolates. J. Bacteriol. 190, 6881–6893.

Ridley, W.P., Kirkwood, S., 1973. The stereospecificity of hydrogen abstraction by uridine diphosphoglucose dehydrogenase. Biochem. Biophys. Res. Commun. 54, 955–960.

Rocha, J., Popescu, A.O., Sa-Correia, I., Fialho, A.M., Frazao, C., 2010a. Cloning, expression, purification, crystallization and preliminary crystallographic

studies of BceC, a UDP-glucose dehydrogenase from Burkholderia cepacia IST408. Acta Crystallogr. F Struct. Biol. Cryst. Commun. 66, 269–271.
Rocha, J., Granja, A.T., Sa-Correia, I., Fialho, A., Frazao, C., 2010b. Cloning, expression, purification, crystallization and preliminary crystallographic studies of UgdG, an UDP-glucose dehydrogenase from Sphingomonas elodea ATCC 31461. Acta Crystallogr. F Struct. Biol. Cryst. Commun. 66, 69–72.
Schiller, J.G., Bowser, A.M., Feingold, D.S., 1973. Partial purification and properties of UDPG dehydrogenase from *Escherichia coli*. Biochim. Biophys. Acta 293, 1–10.
Sommer, B.J., Barycki, J.J., Simpson, M.A., 2004. Characterization of human UDP-glucose dehydrogenase. CYS-276 is required for the second of two successive oxidations. J. Biol. Chem. 279, 23590–23596.
Thompson, J.D., Higgins, D.G., Gibson, T.J., 1994. CLUSTAL W: improving the sensitivity of progressive multiple sequence alignment through sequence weighting, position-specific gap penalties and weight matrix choice. Nucleic Acids Res. 22, 4673–4680.
Wu, K.M., Li, L.H., Yan, J.J., Tsao, N., Liao, T.L., Tsai, H.C., Fung, C.P., Chen, H.J., Liu, Y.M., Wang, J.T., Fang, C.T., Chang, S.C., Shu, H.Y., Liu, T.T., Chen, Y.T., Shiau, Y.R., Lauderdale, T.L., Su, I.J., Kirby, R., Tsai, S.F., 2009. Genome sequencing and comparative analysis of *Klebsiella pneumoniae* NTUH-K2044, a strain causing liver abscess and meningitis. J. Bacteriol. 191, 4492–4501.